ELSEVIER

Surface Science 406 (1998) 90–102

surface science

A photoelectron diffraction study of ordered structures in the chemisorption system Pd{111}-CO

T. Gießel [a], O. Schaff [a], C.J. Hirschmugl [a], V. Fernandez [a], K.-M. Schindler [a], A. Theobald [a], S. Bao [a], R. Lindsay [a], W. Berndt [a], A.M. Bradshaw [a,*], C. Baddeley [b], A.F. Lee [b], R.M. Lambert [b], D.P. Woodruff [c]

[a] *Fritz-Haber-Institut der Max-Planck-Gesellschaft, Faradayweg 4–6, 14195 Berlin, Germany*
[b] *Department of Chemistry, University of Cambridge, Lensfield Road, Cambridge, CB2 1EW, UK*
[c] *Department of Physics, University of Warwick, Coventry, CV4 7AL, UK*

Received 20 November 1997; accepted for publication 14 January 1998

Abstract

The adsorption system Pd{111}-CO gives rise to a series of at least seventeen, sometimes complicated, ordered overlayers. The $(\sqrt{3}\times\sqrt{3})$R30° and c(4×2) phases are formed at coverages of $\theta=0.33$ ML and 0.50 ML, respectively. The results from surface vibrational spectroscopy have hitherto been interpreted in terms of CO adsorbing on threefold symmetric hollow sites in the $(\sqrt{3}\times\sqrt{3})$R30° phase, but occupying bridge sites in the c(4×2) phase. We show in a quantitative photoelectron diffraction study in the scanned energy mode that, whereas hollow sites are indeed occupied in the $(\sqrt{3}\times\sqrt{3})$R30° structure, CO adsorbs in a mixture of fcc and hcp hollows in the c(4×2) phase. Several structural parameters, in particular the Pd-C layer spacings, have been determined. The result is essentially identical to that obtained for the Ni{111}c(4×2)-CO system. It is also inferred that at coverages between 0.33 and 0.50 ML "domain wall", or weakly incommensurate, phases occur in which the percentage of occupied hcp sites increases monotonically as the coverage is raised.

Keywords: Surface structure; Photoelectron diffraction; Chemisorption; Palladium; Carbon monoxide

1. Introduction

Ordered CO structures on transition metal surfaces have been a subject of considerable interest since the pioneering LEED studies of Tracy and Palmberg [1–3]. The splitting and continuous shift of the adsorbate-induced diffraction features which are observed at medium to high coverage were interpreted at the time in terms of a continuous compression of the overlayer to give approximately hexagonal arrays which are no longer in registry with the substrate. A large number of CO structures have since been described with this "out of registry" or "compression" model. Such structures would have to be regarded as strongly incommensurate phases in which the lateral, repulsive interactions in the overlayer become more important than the corrugation of the substrate potential. They are known, for example, in the physisorption of rare gases on graphite at high coverages [4]. Although such models can account qualitatively for the LEED data from many CO systems, they turn out not to be compatible with the correspond-

* Corresponding author. Fax: (+49) 30 8413 5603; e-mail: bradshaw@fhi-berlin.mpg.de

0039-6028/98/$19.00
PII: S0039-6028(98)00098-3

ing vibrational spectra. Pritchard [5] first pointed out that the small number of relatively sharp C–O stretching bands observed for such structures [6], rather than the single broad band which might be expected from a strongly incommensurate system, must be indicative of only a small number of different adsorption sites. For the systems Cu{100}-CO and Cu{111}-CO he proposed that such structures could be better explained in terms of coincident site lattices in which the molecules remain adsorbed in atop and bridge sites. Biberian and Van Hove [7,8] subsequently proposed structural models based on coincident site lattices schemes for a number of CO adsorption systems. They pointed out that such structures may be considered as alternating phase and anti-phase domains separated by walls (or "fault lines") containing CO molecules at a higher local density. The molecules at the domain walls would also be adsorbed on distinct adsorption sites, although the possibility of small lateral displacements [9,10], or of tilting [11], due to strong intermolecular repulsion has also been discussed. Such structures are sometimes described as weakly incommensurate, although equidistant domain walls are not a necessary criterion for this designation.

The adsorption system Pd{111}-CO is particularly interesting in this respect since at least 17 ordered structures have been observed, including two sequences of what might previously have been attributed to "continuous" splittings in the ranges $\theta = 0.33$–0.50 ML and 0.50–0.60 ML [12,13]. At $\theta = 0.33$ and 0.50 ML the observed LEED patterns correspond to $(\sqrt{3} \times \sqrt{3})$R30° and c(4 × 2) ordered arrays (or in an alternative, and for present purposes perhaps more useful, notation [7,8] c($\sqrt{3} \times 3$)rect and ($\sqrt{3} \times 2$)rect, respectively). The IR reflection–absorption spectra show single vibrational bands at 1848 cm^{-1} and at 1920 cm^{-1}, respectively, with halfwidths of ≈ 10 cm^{-1} [12,13]. In the original interpretation of the IR data [14] the $(\sqrt{3} \times \sqrt{3})$R30° structure was assigned to CO adsorbed in threefold hollow sites (later confirmed in an early quantitative LEED study [15]) and the c(4 × 2) structure to CO in bridge sites (see Fig. 1a and 1c). The C–O stretching frequency at $\theta =$ 0.50 ML corresponds roughly to that expected from a bridging species. Moreover, the CO molecules are equidistant in this structural model which, if lateral interactions are important, is expected to be the most likely configuration. The transition from $(\sqrt{3} \times \sqrt{3})$R30° to c(4 × 2) as a function of increasing coverage then occurs via a sequence of at least five identifiable ordered structures which can be envisaged in terms of the introduction of equally spaced domain walls in the ⟨211⟩ direction at which CO adsorbs on bridge sites at a higher local coverage. This is shown in Fig. 1b for the ($\sqrt{3} \times 5$)rect structure. A similar explanation would then apply to the transition between the c(4 × 2), or ($\sqrt{3} \times 2$)rect, structure at $\theta = 0.50$ ML and the c($\sqrt{3} \times 5$)rect structure at $\theta = 0.60$ ML which also involves five identifiable domain wall structures [12].

The system Ni{111}-CO is also characterised by a c(4 × 2) structure at half-coverage, although apart from a recently reported diffuse (2 × 2) structure [16] this is the only ordered overlayer reported for $\theta < 0.5$ ML. On the basis of vibrational spectra it was also originally thought that after initial adsorption in threefold symmetric hollow sites, bridge sites are occupied at higher coverage [17]. In fact, adsorption continues to occur in hollow sites up to a coverage of 0.50 ML, the c(4 × 2) structure consisting of equal numbers of CO molecules in the so-called fcc and hcp sites [18]. The question must then be posed as to whether the c(4 × 2) structure, and indeed the two sequences of domain wall structures, on Pd{111} also consist of CO molecules adsorbed only in hollow sites. The corresponding structure models for the $(\sqrt{3} \times \sqrt{3})$R30°, ($\sqrt{3} \times 5$)rect and c(4 × 2) phases are shown in Fig. 1, parts (a), (d) and (e), respectively. For this reason we have investigated quantitatively with scanned energy mode photoelectron diffraction [19] the $(\sqrt{3} \times \sqrt{3})$R30° and c(4 × 2) structures. A brief account of part of this work has already appeared [20].

Photoelectron diffraction in the scanned energy mode involves the measurement of an adsorbate core-level photoelectron line at a pre-selected emission angle as a function of photon energy, and thus of photoelectron energy [19]. (Clearly, synchrotron radiation is required for this experiment,

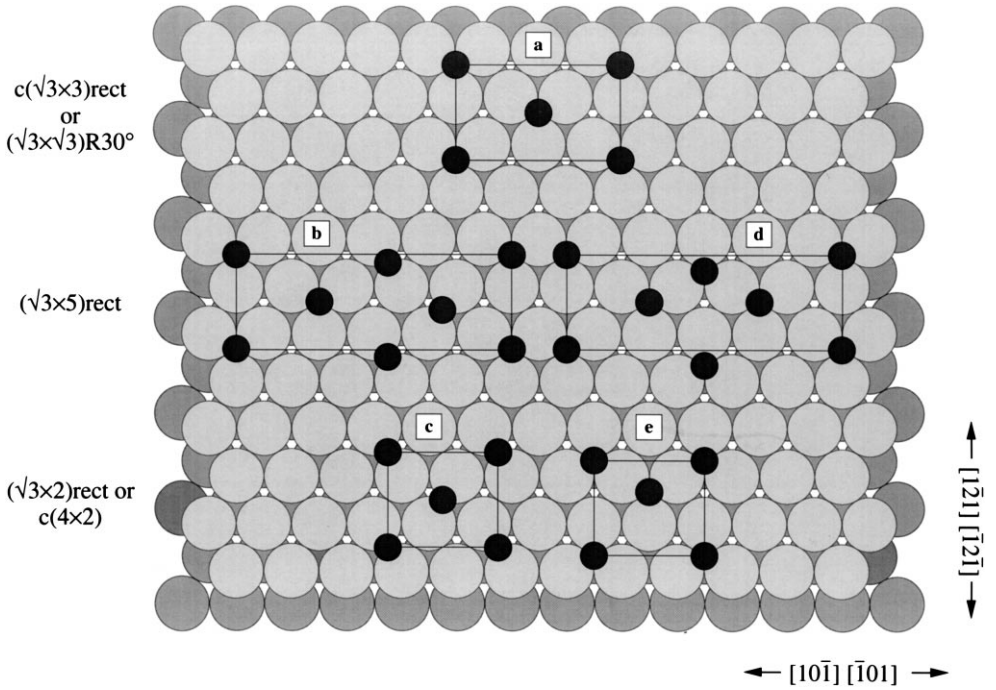

Fig. 1. Two models for the transition from the $(\sqrt{3}\times\sqrt{3})$R30°, or $(\sqrt{3}\times 3)$rect, phase of CO on Pd{111} at $\theta=0.33$ ML to the $c(4\times 2)$, or $(\sqrt{3}\times 2)$rect, phase at $\theta=0.50$ ML via a sequence of weakly incommensurate phases. As an example of the latter the $(\sqrt{3}\times 5)$rect structure is shown. In the first model depicted in a, b and c, equidistant domain walls in the $\langle 211\rangle$ direction with the CO molecules occupying bridge sites are introduced. Increasing coverage results in the $c(4\times 2)$ structure containing only bridge sites. In the second model depicted in a, d and e, CO molecules occupying hcp-hollow sites are introduced. With increasing coverage a 1:1 mixture of hcp- and fcc-hollow sites results at $\theta=0.50$ ML.

since conventional soft X-ray sources for photoelectron spectroscopy have a fixed photon energy.) The dependence of photoelectron intensity on kinetic energy is modulated by the interference between the directly emitted component of the photoelectron wave and the components that arise from elastic scattering at the neighbouring substrate atoms. The modulations depend in turn on the respective path length differences and thus provide information on the local geometry of the emitter atom. The latter is extracted in a similar way to LEED by comparing experimental "modulation functions" with simulated curves calculated using multiple scattering theory.

2. Experimental details and data analysis

The experiments were performed in a purpose-built ultra-high vacuum system on the HE-TGM-1 monochromator [21] at the BESSY synchrotron radiation source. A 152 mm mean radius 150° electrostatic deflection analyser with three parallel channeltrons (VG Scientific) was used to measure the photoelectron diffraction signal at a fixed angle of 60° relative to the photon incidence direction. The Pd{111} sample was prepared by the usual methods of orientation with Laue X-ray diffraction, spark machining, polishing and in situ cleaning with argon bombardment and anneal cycles. In order to remove carbon completely, it was found necessary to perform occasional oxygen treatments (300 s at 5×10^{-8} mbar and 850 K). After such a treatment a well-defined (1×1) LEED pattern was observed. Atomic cleanness was monitored with photoelectron spectroscopy using synchrotron radiation. Both the $(\sqrt{3}\times\sqrt{3})$R30° and $c(4\times 2)$ phases were prepared by dosing CO (purity, 99.999%) from the gas phase. A sharp $(\sqrt{3}\times\sqrt{3})$R30° LEED pattern was obtained after

dosing 0.85×10^{-6} mbar s of CO at 200 K. The sharpest c(4×2) pattern was achieved after dosing 2.25×10^{-6} mbar s CO at 200 K. The c(4×2) pattern was always less sharp than the $(\sqrt{3}\times\sqrt{3})$R30° and vanished in the electron beam after about 60 s. It also proved difficult to prepare the c(4×2) phase again in exactly the same quality for each photoelectron diffraction scan. Thus, several of the modulation functions, or parts of a particular modulation function, may actually have been measured for one or more of the weakly incommensurate structures at lower and at higher coverages on each side of the c(4×2) structure. This turns out not to be particularly important, as is discussed in Sections 4.2 and 5.

The C 1s photoelectron diffraction spectra were taken at a temperature of 130 K at polar angles between 0° and 60°, in steps of 10°, in all three principal azimuths for both phases. The signal was recorded at successive photon energies (separated by 2 eV) for kinetic energies of about ±20 eV around the C 1s core level peak to give the energy distribution curves (EDCs). The intensity of each of these peaks was then determined by background subtraction and integration, and the resulting intensity–energy spectra were normalised to give the modulation functions [22] defined by

$$\chi_{ex}(\theta,\phi,k)=\frac{I(\theta,\phi,k)-I_0(\theta,\phi,k)}{I_0(\theta,\phi,k)}, \qquad (1)$$

where I and I_0 are the diffractive and non-diffractive intensities, θ and ϕ are the polar and azimuthal emission angles and k is the modulus of the photoelectron wavevector. Unfortunately, it is not possible at present to measure the corresponding O 1s modulation functions because the O 1s photoelectron line has almost the same binding energy as the Pd $3p_{3/2}$ feature at 532 eV.

The particular problems encountered with palladium as a substrate are illustrated in Fig. 2a which shows the C 1s photoelectron line of CO adsorbed on Pd{111} at $\theta=0.50$ ML plotted successively in steps of 8 eV photon energy on a kinetic energy scale. (As mentioned above the spectra were actually recorded in steps of 2 eV; for purposes of illustration only every fourth is shown.) The inset in Fig. 2a is an expanded-scale view of the range

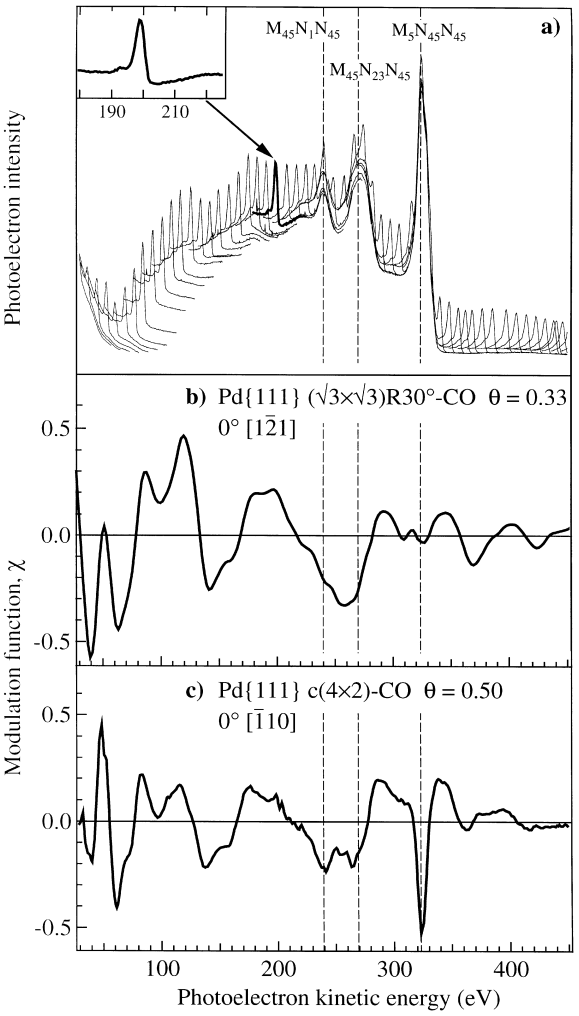

Fig. 2. (a) C 1s photoelectron diffraction spectrum from Pd{111}c(4×2)-CO recorded in normal emission; individual C 1s photoelectron energy distribution curves are shown at successively higher photon energies (separated by 8 eV for better illustration of the principle). Note the intense Pd Auger lines, on which the successive C 1s spectra are superimposed. (b) Modulation function extracted from the C 1s data recorded in normal emission for Pd{111}$(\sqrt{3}\times\sqrt{3})$R30°-CO. (c) Modulation function extracted from the C 1s data recorded in normal emission for Pd{111}c(4×2)-CO; note the strong artifacts in the energy range of the Pd Auger lines.

180–225 eV and illustrates this principle more clearly. In contrast to the situation for Ni surfaces, the underlying Auger transitions are at least a factor of 10 stronger than the intensity modulations [20]. The fact that we have been able to

analyse the data and obtain reasonable modulation functions (e.g. Fig. 2b) is due to the development of new integration routines. These involve fitting each EDC with a Gaussian function, a Gaussian-broadened step function and a background template. The latter is obtained from the overlapping high energy ends of the EDCs. The intensity is then taken as the area under the Gaussian function. The procedure worked reasonably well in the region of the strongest Auger transitions for the $(\sqrt{3}\times\sqrt{3})$R30° data set, so that the "whole" 30–480 eV range of the modulation functions could be used in the analysis. The $c(4\times2)$ data sets have been measured in a second beam time at somewhat lower resolution, giving rise to various artifacts in the Pd Auger region (e.g. Fig. 2c). In this case only the energy range 30–230 eV was used for comparison with the simulations.

3. Simulations

In our normal approach [19,22] quantitative structure determination generally proceeds in two stages. A direct method is used to determine the adsorption site employing the full set of data and calculating the "projection integrals" [23,24]. The underlying physical principle is that modulation functions measured in directions which correspond to 180° scattering from a near-neighbour substrate atom ("the backscattering geometry") are typically dominated by this event and show particularly strong intensity modulations. Such a modulation function can thus be described within the single scattering approximation with only one scatterer taken into account. The method produces a three-dimensional intensity map of the space around the emitter, with maximum values of the "projection integral" in regions corresponding to the nearest neighbour backscatterers. The second stage is a full quantitative structural analysis using an iterative "trial-and-error" procedure which involves a comparison of a reduced set of usually 6–8 experimental spectra with the results of multiple scattering simulations based on trial model structures. These calculations have been performed on the basis of an expansion of the final state wavefunction into a sum over all scattering pathways which the electron can take from the emitter atom to the detector outside the sample. A magnetic quantum number expansion of the free electron propagator has been used to calculate the scattering contribution of an individual scattering path [25,26]. Double and higher order scattering events were treated by means of the reduced angular momentum expansion [27]. The finite energy resolution and angular acceptance of the electron analyser are included. Anisotropic vibrations for the emitter atom and isotropic vibrations for the scattering atoms are also taken into account. The comparison between theory and experiment is aided by the use of a reliability factor

$$R_{\mathrm{m}} = \sum (\chi_{\mathrm{th}} - \chi_{\mathrm{ex}})^2 / \sum (\chi_{\mathrm{th}}^2 + \chi_{\mathrm{ex}}^2), \qquad (2)$$

where a value of 0 corresponds to perfect agreement, a value of 1 to uncorrelated data, and a value of 2 to anticorrelated data [19,22]. The search in parameter space to locate the structure having the minimum R factor was helped by the use of a Marquardt algorithm, in which the calculation of the curvatures is made considerably faster by using the so-called linear method [28].

In order to estimate the errors associated with the individual structural parameters we use an approach based on that of Pendry which was derived for LEED [29]. This involves defining a variance in the minimum of the R factor, R_{min} as

$$\mathrm{Var} = R_{\mathrm{min}} \sqrt{2/N}, \qquad (3)$$

where N is the number of independent pieces of structural information contained in the set of modulation functions used in the analysis. All parameter values giving structures with R factors less than $R_{\mathrm{min}} + \mathrm{Var}(R_{\mathrm{min}})$ are regarded as falling within one standard deviation of the "best fit" structure. More details of this approach, in particular on the definition of N, can be found in a recent publication [30].

4. Results

4.1. The $(\sqrt{3}\times\sqrt{3})R30°$ structure

Fig. 3 shows the result of the application of the projection method to the complete data set for the

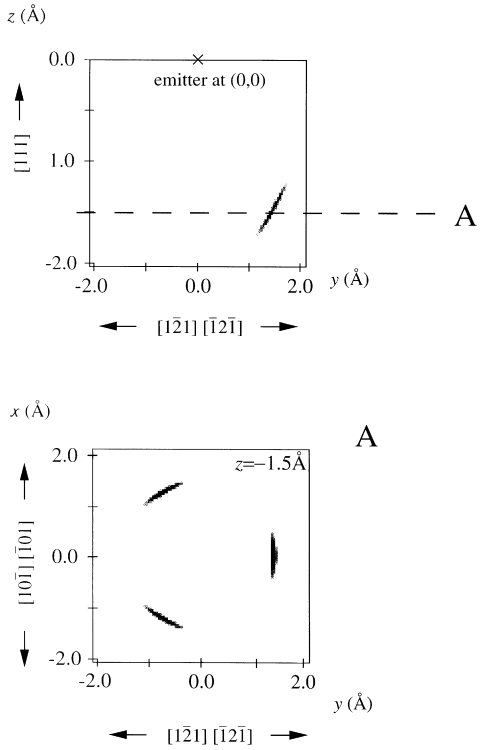

Fig. 3. Image side and top view of the nearest-neighbour substrate atoms of the C emitter atom for the Pd{111}($\sqrt{3}\times\sqrt{3}$)R30°-CO phase obtained by application of the projection method to the C 1s spectra. The azimuthal orientation in the x–y plane leads to the conclusion that fcc-hollow sites are occupied.

Pd{111}($\sqrt{3}\times\sqrt{3}$)R30°-CO phase. As described in Section 2, such grey-scale plots can be regarded as images of the nearest-neighbour substrate atoms. Two cuts through a cube in real space directly "below" the emitting atom are shown. In the top panel the cut is perpendicular to the surface through the emitter in a ⟨211⟩ azimuth; in the bottom panel the cut is parallel to the surface, but 1.5 Å below the emitter. From the threefold rotational symmetry of the pattern and the separation between the emitter and the three features, it is immediately clear that the carbon atom, and thus the CO molecule, occupies a hollow site. Furthermore, from the azimuthal orientation of the threefold pattern relative to the known azimuthal orientation of the crystal during the measurements it can be ascertained that the so-called fcc hollow site is occupied. The latter is the hollow site with a Pd atom directly beneath in the third layer as opposed to that with a Pd atom directly beneath in the second layer ("hcp" site). This agrees completely with the site determination in the LEED study of Ohtani et al. [15]. The structural model in Fig. 4 is drawn such that it can be directly compared with the bottom panel of Fig. 3.

Having established the surface site and the approximate vertical distance of the emitter above the outermost Pd layer, we can now perform the quantitative structural analysis using the trial-and-error scheme, but in a much reduced parameter space. The C 1s modulation functions for the eight different emission directions used in the analysis are shown as bold curves in Fig. 5. (Note that

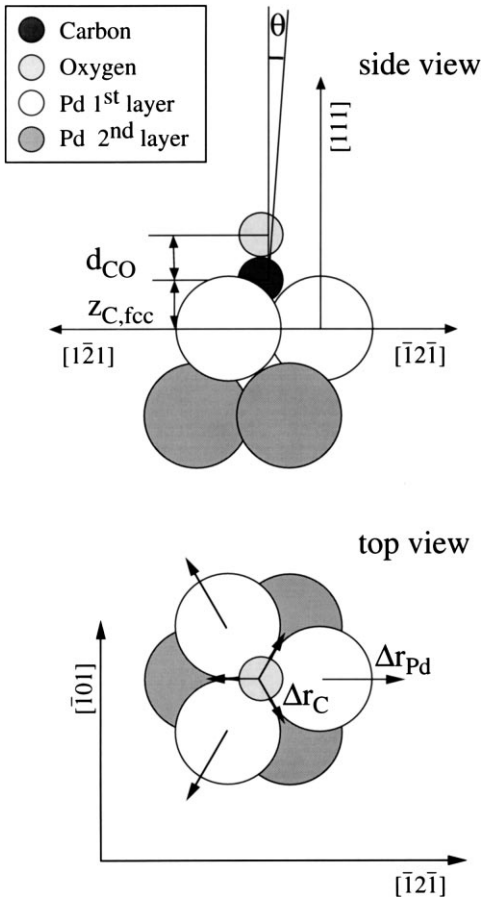

Fig. 4. Scheme of the local adsorption geometry of the CO molecule in the Pd{111}($\sqrt{3}\times\sqrt{3}$)R30°-CO structure.

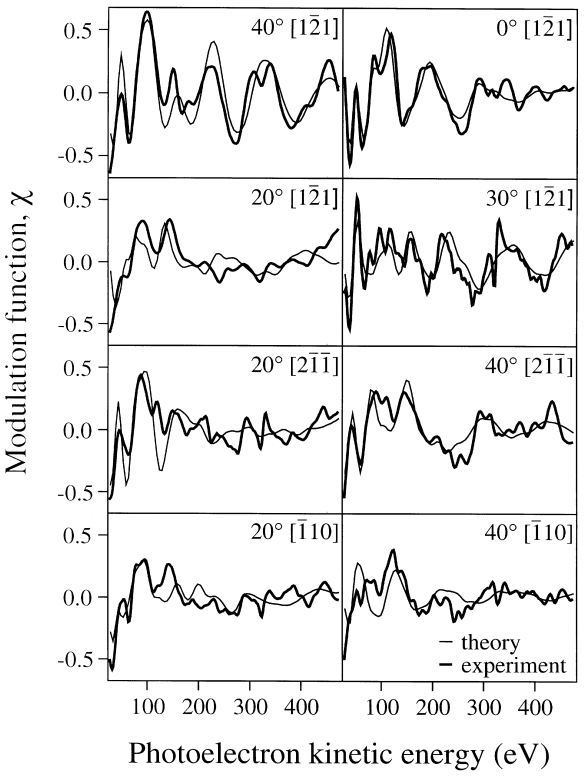

Fig. 5. Comparison of experimental and calculated C 1s modulation functions for the Pd{111}($\sqrt{3}\times\sqrt{3}$)R30°-CO structure.

there is still some remnant of the strongest Auger feature just above 300 eV in most of the curves.) The parameters varied are the C–Pd vertical layer spacing, $z_{C,fcc}$, as well as the lateral displacements of the carbon atom and the three Pd atoms forming the adsorption site, Δr_C and Δr_{Pd}, respectively (Fig. 4). Certain parameters which are relatively ineffective in reducing the R factor were not varied. The first Pd–Pd layer separation, for instance, was maintained at the bulk value of 2.25 Å.

The best fit is obtained for the values of the three parameters given in Table 1. The corresponding calculated modulation functions are shown as the faint curves in Fig. 5. The overall eight-spectrum R factor is $R_m = 0.24$; the R factors for the individual spectra are 0.14, 0.14, 0.37, 0.25, 0.36, 0.20, 0.31 and 0.57 for the 40°, 0°, 20° and 30° polar angles in the [1$\bar{2}$1] azimuth, 20° and 40° in the [2$\bar{1}\bar{1}$] azimuth and 20° and 40° in the [$\bar{1}$10] azimuth, respectively. Note that the best agreement between theory and experiment is obtained for normal emission and for the favoured backscattering geometry (i.e. 40° in [1$\bar{2}$1]) in which there is a Pd substrate atom directly "behind" the emitter. This leads to a dominant single oscillation in the modulation function and good agreement between the experimental and simulated curves. The carbon–Pd layer separation of $z_{C,fcc} = 1.27(\pm 0.05)$ Å agrees very well with the LEED value of 1.29($\pm$0.05) Å [18]. Δr_{Pd} and Δr_C are, as expected, essentially zero, although the error bars here are $\pm$0.10 Å. The Pd–C bondlength is 2.03($\pm$0.04) Å. Not given in Table 1 are the values of $d_{CO} = 1.25(+0.14/-0.11)$ Å and $\theta = 0(\pm 23)°$ for the C–O bond length and the C–O tilt angle, respectively, since these can only be determined approximately from the C 1s data set. The scattering from the oxygen atom is much weaker than that from the Pd substrate and essentially in the forward direction. Normally, the combination of O 1s and C 1s data sets would give these parameters relatively accurately, e.g. Ref. [31]; as noted above, however, it has so far not been possible to

Table 1
Optimised values of the position parameters

Parameter	($\sqrt{3}\times\sqrt{3}$)R30° phase		c(4×2) phase
	Optimum value (present work)	Optimum value, Ohtani et al. [15]	Optimum value (present work)
$z_{C,fcc}$	1.27($\pm$0.05) Å	1.29($\pm$0.05) Å	1.31($\pm$0.06) Å
$z_{C,hcp}$			1.37($\pm$0.06) Å
$d_{Pd-C,fcc}$	2.03($\pm$0.04) Å	2.05($\pm$0.04) Å	2.06($\pm$0.04) Å
$d_{Pd-C,hcp}$			2.10($\pm$0.04) Å
Δr_{Pd}	0.00($\pm$0.10) Å	0.00 Å	
Δr_C	0.01($\pm$0.10) Å		

measure the corresponding O 1s modulation functions.

4.2. The c(4×2) structure

Unfortunately, the projection method did not give consistent results for this phase (see discussion in Section 5) so that in the absence of preliminary information on the adsorption site(s) a different strategy was adopted for the structural determination. Simulations were performed for all possible highly symmetric adsorption sites compatible with the c(4×2) mesh; the latter are shown in Fig. 6. Eight C 1s modulation functions were used and are shown as bold curves in Fig. 7; as explained above, the modulation functions were truncated at 230 eV. In order to reduce the computational time in this first stage to an acceptable level, the only parameters that were optimised for each local geometry (or combination of local geometries) were the vertical layer separations for different adsorption sites separately, $z_C(1)$ and $z_C(2)$. It was assumed that the C–O axis is perpendicular and that the molecule bonds to the surface via the C atom. The resulting overall R factors are given in the first column in Table 2 and reveal that the most probable structure consists of a mixture of fcc and hcp hollow sites ($R_m = 0.28$), but that the R factor of any structure involving hollow sites is also relatively low (0.36–0.46). Of the latter, the R factors for the mixtures involving the fcc hollow sites are lower than those involving the hcp hollow sites.

In the second stage of the optimisation procedure, a full trial-and-error analysis was performed for all structures involving the fcc hollow sites (C, G, E and I) but, in order to reduce the computational time, using only four of the modulation functions in Fig. 7, namely, 35° [$\bar{1}$10], 10° [$\bar{1}$10], 50° [1$\bar{2}$1] and 40° [2$\bar{1}\bar{1}$]. These directions were chosen because they were most sensitive to the different combinations of adsorption sites as found in the optimisation of $z_C(1)$ and $z_C(2)$ in the first stage of analysis. The optimised parameters were: the C–Pd layer spacings, $z_C(1)$ and $z_C(2)$; the C–O bondlengths, $d_{CO}(1)$ and $d_{CO}(2)$,

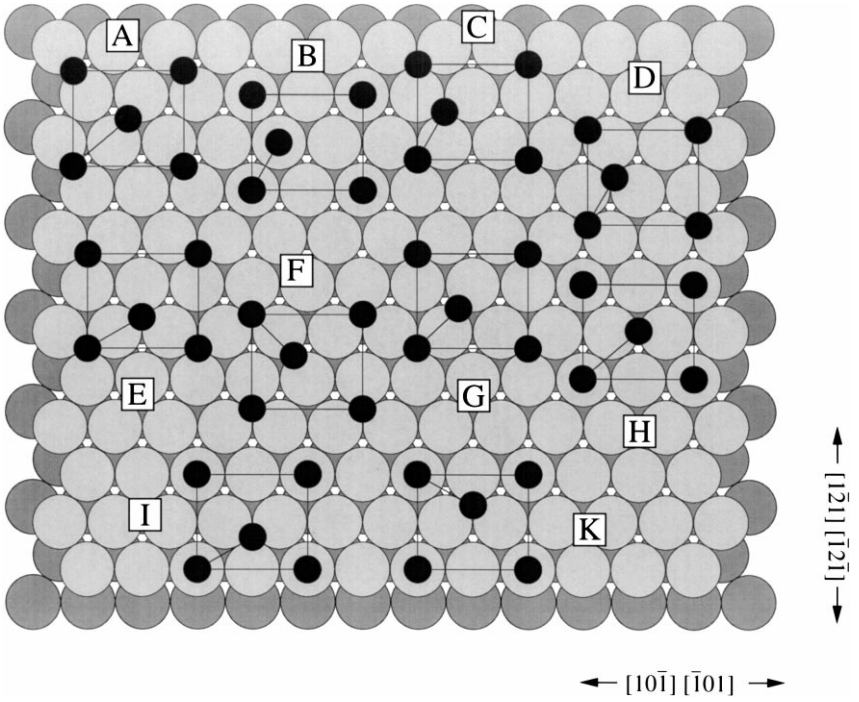

Fig. 6. Initial trial geometries investigated for the Pd{111}c(4×2)-CO structure.

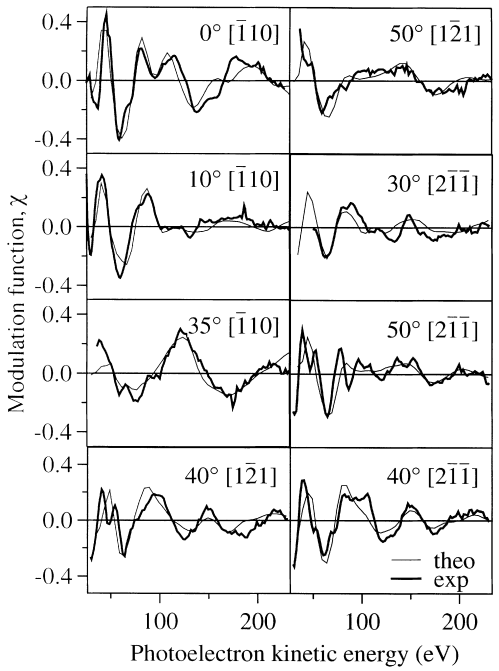

Fig. 7. Comparison of experimental and calculated C 1s modulation functions for the Pd{111}c(4×2)-CO structure.

for each of the two CO molecules and the mixing ratio of different adsorption sites.

The lateral displacement of the Pd atoms Δr_{Pd} forming the hollow sites which had been optimised for the $(\sqrt{3}\times\sqrt{3})R30^\circ$ structure was not varied because in most of the trial structures at least one Pd atom is common to each group of atoms forming the surface sites for the two CO molecules. The lateral displacement of the C atom Δr_C was also not taken into account because this would have unreasonably increased the calculation time owing to the large number of energetically equivalent domains. Instead, the anisotropic vibrational amplitude of the emitter has been optimised (but assumed to be the same for both molecules). This approach is similar to optimising lateral shifts Δr_C since a small shift away from a highly symmetric site can be equally well described by an increased lateral vibrational amplitude of the emitter adsorbed in the high-symmetry site. This effect is similar to the concept of "split positions" in LEED [32] and has also been observed recently in PhD structural analysis [33,34]. All parameters used in the analyses of the c(4×2) structure were optimised simultaneously apart from the tilt angle of the C–O axis with respect to the surface normal which was determined subsequently in an additional simulation.

The resulting *R* factors are given in the second column of Table 2; the best value of 0.17 was obtained for the fcc/hcp hollow mixture. All other *R* factors lie outside the variance of 0.03. In the third stage, all parameters were again fully optimised for the fcc/hcp hollow mixture, but using all eight modulation functions shown in Fig. 7. The Pd–C bondlengths are 2.06(±0.04) Å (fcc) and 2.10(±0.04) Å (hcp). The resulting *R* factor was 0.20; the structural parameters are given in Table 1, the local adsorption geometry is depicted in Fig. 8 and the corresponding simulated modulation func-

Table 2
Best *R* factors obtained from preliminary and final optimizations carried out for the Pd{111}c(4×2)-CO structure

	Adsorption site	*R* factor		
		1st stage	2nd stage	3rd stage
A	bridge	0.72		
B	atop	0.67		
C	fcc hollow	0.39	0.35	
D	hcp hollow	0.46		
E	fcc hollow and hcp hollow	0.28	0.17	0.20
F	bridge and fcc hollow	0.45		
G	bridge and fcc hollow	0.38	0.23	
H	bridge and atop	0.59		
I	fcc hollow and atop	0.36	0.33	
K	hcp hollow and atop	0.44		

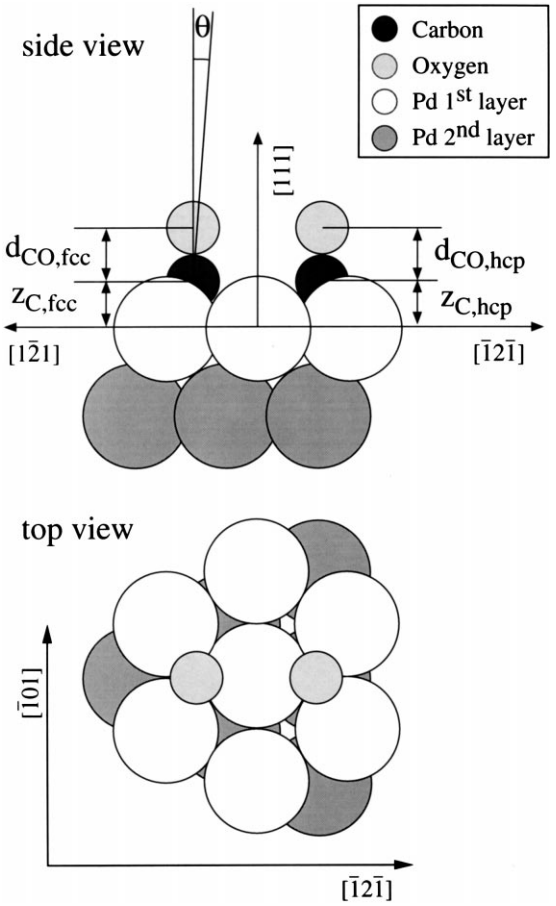

Fig. 8. Scheme of the local adsorption geometry of the two CO molecules in the primitive unit cell of the Pd{111}c(4×2)-CO structure.

tions are also shown in Fig. 7. The individual R factors for the different modulation functions are 0.14, 0.30, 0.22, 0.19, 0.22, 0.35, 0.15 and 0.12 for the 0°, 40° and 50° polar angles in the [1$\bar{2}$1] azimuth, 0°, 40° and 50° in the [2$\bar{1}\bar{1}$] azimuth and 10° and 35° in the [$\bar{1}$10] azimuth, respectively. The optimised value for the fraction of fcc sites is 56(±19)%. Note that $z_{C,fcc}$ is larger in the c(4×2) phase than in the $(\sqrt{3}\times\sqrt{3})$R30° phase, although the difference is inside the error bars. In the case of the hcp site, however, the increase is definitely significant. d_{CO} for fcc and hcp are 1.14(±0.12) Å and 1.14(±0.14) Å, respectively; the angle of inclination is 0(±25)°. Again, we emphasise that the latter values would normally be determined using a combination of data from both core levels and not from C 1s modulation functions alone. The optimised values for the mean square amplitudes of vibration of the C atom parallel and perpendicular to the surface are $32.8\times10^{-3}(\pm21.0\times10^{-3})$ Å^2 and $6.4\times10^{-3}(\pm4.3\times10^{-3})$ Å^2, respectively. The mean square amplitude of vibration of both the bulk and surface atoms of the substrate was estimated from the Debye temperature to be 2.5×10^{-3} Å^2. Despite the large error bars we note that the amplitude for the lateral vibrations is considerably larger than for the vibrations perpendicular to the surface. This might be an indication that the emitter atoms are slightly shifted away from the centres of the hollow sites in order to reduce the lateral repulsion. In structure E the lowest CO–CO distance is 3.18 Å compared with 3.64 Å in structure A (where the CO molecules are equidistant).

In order to investigate the possibility of such shifts we have introduced four more parameters for the lateral movement of each of the two molecules in a subsequent simulation. Isotropic vibrations of the emitter were, however, assumed and, in order to keep the computational time feasible, intermolecular scattering was omitted. The R factor improved only marginally to 0.20 from 0.21 for a reference optimisation under the same conditions but with the CO molecules fixed in the centres of the hollow sites. The maximum lateral deviation from the hollow sites was 0.14 Å. Since the improvement in the R factor is much smaller than the variance (var=0.03) such lateral shifts remain possible, but the present data do not indicate that they are significant.

5. Discussion

The present results show that, in contrast to the previous interpretation of the LEED and IR data [12,14,35,36], bridge sites are not occupied in the c(4×2) phase. Adsorption occurs initially in fcc threefold symmetric hollow sites and, at $\theta=$ 0.50 ML in the c(4×2) phase, approximately equal numbers of fcc and hcp hollow sites are filled. By inference, therefore, the model of Fig. 1d for the sequence of structures must pertain. The

mechanism by which the change in coverage occurs is best envisioned by starting with the $(\sqrt{3}\times\sqrt{3})$R30° structure at $\theta=0.33$ ML and introducing equally spaced domain walls running along the $\langle 211\rangle$ direction with CO molecules adsorbed in hcp hollow sites. This is shown in Fig. 1d for the $(\sqrt{3}\times 5)$rect structure where the fcc:hcp ratio is 3:1. Eventually the c(4×2) structure is reached when the fcc:hcp ratio is 1:1. Altogether five ordered structures have been identified in this coverage range [13]. It is possible that more ordered structures occur in this sequence and could perhaps be observed if the experiment were to be performed at a lower temperature [12]. The single C–O stretch at $\approx 1920\ \mathrm{cm}^{-1}$ in the c(4×2) structure is due to an array of CO molecules (in two different sites and with two distinct separations). The absorption band is shifted by $72\ \mathrm{cm}^{-1}$ relative to that of the $(\sqrt{3}\times\sqrt{3})$R30° structure and by $\approx 120\ \mathrm{cm}^{-1}$ relative to the zero coverage limit. At coverages between 0.33 and 0.50 ML, corresponding to the $(\sqrt{3}\times\sqrt{3})$R30° and c(4×2) structures, the IR spectrum consists of typically three, partly resolved bands, at about $1840\ \mathrm{cm}^{-1}$, $1880\ \mathrm{cm}^{-1}$ and $1910\ \mathrm{cm}^{-1}$ which are broader than those observed for the two commensurate structures ($\approx 10\ \mathrm{cm}^{-1}$). In a forthcoming paper we discuss the IR spectra and the various ordered structures in more detail [13].

In the corresponding system Ni{111}-CO no $(\sqrt{3}\times\sqrt{3})$R30° structure is formed at $\theta=0.33$ ML [17], although a (2×2) structure at $\theta\approx 0.25$ ML has recently been reported [16]. In this phase, a mixture of fcc and hcp hollow sites is occupied with $z_{\mathrm{C,hcp}}=1.26(\pm 0.04)$ Å and $z_{\mathrm{C,fcc}}=1.30(\pm 0.08)$ Å; the proportion of hcp sites is $64(\pm 22)$%. The error bars on the layer spacings both in these and the present data are thus too large to make any meaningful comparison of bond lengths. The vibrational frequency at $\theta\approx 0.33$ ML in the Ni{111}-CO system is somewhat higher at $\approx 1880\ \mathrm{cm}^{-1}$ [17] compared with $1848\ \mathrm{cm}^{-1}$ in Pd{111}-CO. It is also not possible to measure at present the other interesting structural parameter, d_{CO}, with the necessary accuracy for comparison with the free molecule or with other systems, even in cases where the O 1s modulation functions are available [31]. This also applies to most quantitative LEED investigations where d_{CO} is also typically given with an error bar of ± 0.05 Å.

We now discuss some of the implications of the present data for photoelectron diffraction studies in general. The Pd MNN Auger structures in the raw data of Fig. 2 are at least a factor of 10 stronger than the intensity modulations. The fact that it is possible to perform quite reasonable integrations is remarkable. As noted above, the higher the resolution, the less chance there is of obtaining artifacts from the Auger structures. This was noticed not only in the comparison of the $(\sqrt{3}\times\sqrt{3})$R30° and c(4×2) data sets, but also in the c(4×2) data itself: in two spectra (50° [$1\bar{2}1$], 35° [$\bar{1}10$]) the C 1s halfwidth was 2.1–3.5 eV and thus ≈ 0.4 eV narrower than in the other spectra. The main artifact at about 330 eV is considerably less pronounced in these two modulation functions. Moreover, data taken at the Advanced Light Source in Berkeley for CO on Pd{110} at an experimental resolution of 0.7 eV show almost no artifacts at all [37]. For successful integration it is clearly necessary that the linewidth of the adsorbate feature be much narrower than that of the Auger transitions. This general problem will be encountered with almost all second row transition metals because of strong MNN Auger lines in the kinetic energy region below 400 eV.

That the projection method was unable to give a consistent result for the c(4×2) phase is surprising since it works quite well not only for the $(\sqrt{3}\times\sqrt{3})$R30° phase on this surface, but also for the c(4×2)-CO structure on Ni{111} [18]. Indeed, this is one of the very few examples we have found so far where the projection method fails to give a sensible answer for a symmetric adsorption site, or rather a combination of symmetric adsorption sites. Apart from the truncation of the modulation functions due to the background problems associated with the Auger lines, there is another reason for the problems associated with the projection method: We note that there are significant differences in the scattering amplitudes for Pd and Ni. Fig. 9 shows the modulus of the scattering amplitude $|f|$ for Pd and Ni as a function of the electron kinetic energy and the scattering angle in the

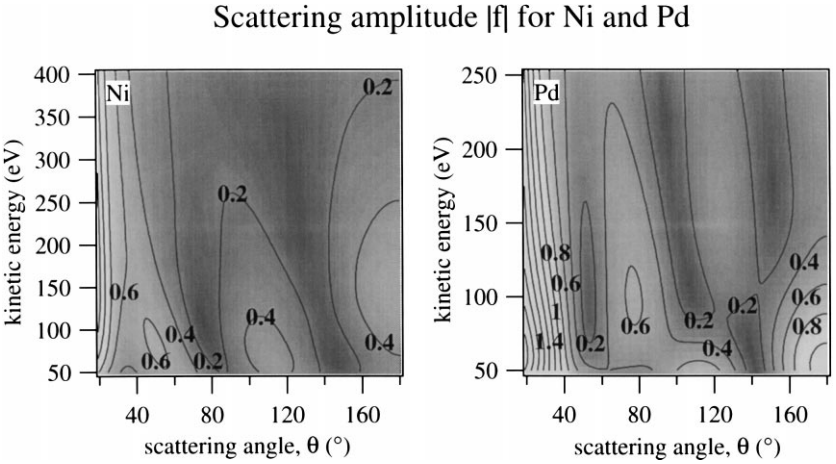

Fig. 9. Comparison of the modulus of the scattering factor $|f|$ for Ni and Pd.

energy ranges used. Pd shows additional maxima at scattering angles of about 80° and 130° which are present over the whole energy range 50–220 eV. In the case of Ni these maxima are less pronounced and, of course, the energy range is greater. Thus, in the case of Pd the criterion for the successful application of the projection method, i.e. that the strongest scattering apart from the forward direction is in the 180° backscattering direction, is not fulfilled. In the $(\sqrt{3}\times\sqrt{3})$R30° case the energy range is greater and, in addition, there is only one adsorption site and correspondingly fewer domains.

6. Conclusions

In the $(\sqrt{3}\times\sqrt{3})$R30°-CO structure formed at $\theta=0.33$ ML on Pd{111} the CO molecules are found to occupy fcc threefold symmetric hollow sites with a C–Pd layer spacing of 1.27($\pm$0.05) Å. The result agrees well with a relatively early LEED determination. There are essentially no lateral displacements of either the C atom or the three Pd atoms forming the hollow site. The c(4×2) structure is found to consist of equal numbers of CO molecules in fcc and hcp hollow sites with C–Pd layer spacings of 1.31($\pm$0.06) Å and 1.37($\pm$0.06) Å, respectively. In the interpretation of data from surface vibrational spectroscopy it had previously been assumed that a switching occurs from the hollow site at $\theta=0.33$ ML to the bridge site at $\theta=0.50$ ML. The C–O stretching frequencies at the two coverages are 1848 cm^{-1} and 1920 cm^{-1}, respectively. The complex domain wall structures occurring between these two coverages (there are at least five) are accompanied by a monotonic increase in the occupation of hcp hollow sites. The data also show that it is possible to carry out quantitative structural analyses for adsorbates on second row transition metal surfaces despite the presence of extremely intense Auger lines which are at least a factor of ten stronger than the photoelectron diffraction intensity modulations.

Acknowledgements

The authors are pleased to acknowledge Volker Fritzsche for his provision of the multiple scattering codes used in this work, and financial support in the form of grants from the European Community HCM Networks (grant ERB CHRX CT930358) and Large-Scale Facilities programmes, the German Federal Ministry of Education, Science, Research and Technology (contract no. 05 625EBA 6) and the Engineering and Physical Sciences Research Council (UK).

References

[1] J.C. Tracy, P.W. Palmberg, J. Chem. Phys. 51 (1969) 4582.
[2] J.C. Tracy, J. Chem. Phys. 56 (1972) 2736.
[3] J.C. Tracy, J. Chem. Phys. 56 (1972) 2748.
[4] P. Bak, Rep. Prog. Phys. 45 (1982) 586.
[5] J. Pritchard, Surf. Sci. 79 (1979) 231.
[6] N. Sheppard, T.T. Nguyen, Adv. IR Raman Spectrosc. 5 (1978) 67.
[7] J.P. Biberian, M.A. Van Hove, Surf. Sci. 118 (1982) 443.
[8] J.P. Biberian, M.A. Van Hove, Surf. Sci. 138 (1984) 361.
[9] T. Uvdahl, P.-A. Karlsson, C. Nyberg, S. Andersson, N.V. Richardson, Surf. Sci. 202 (1988) 167.
[10] B.N.J. Persson, M. Tüshaus, A.M. Bradshaw, J. Chem. Phys. 92 (1990) 5034.
[11] M. Kiskinova, A. Szabo, J.T. Yates, Surf. Sci. 205 (1988) 215.
[12] M. Tüshaus, W. Berndt, H. Conrad, A.M. Bradshaw, B. Persson, Appl. Phys. A 51 (1990) 91.
[13] M. Tüshaus, W. Berndt, T. Gießel, A.M. Bradshaw, to be published.
[14] A.M. Bradshaw, F.M. Hoffmann, Surf. Sci. 72 (1978) 513.
[15] H. Ohtani, M.A. Van Hove, G.A. Somorjai, Surf. Sci. 187 (1987) 372.
[16] R. Davis, D.P. Woodruff, Ph. Hofmann, O. Schaff, V. Fernandez, K.-M. Schindler, V. Fritzsche, A.M. Bradshaw, J. Phys.: Condens. Matter 8 (1996) 1367.
[17] L. Surnev, Z. Xu, J.T. Yates Jr., Surf. Sci. 201 (1988) 1.
[18] K.-M. Schindler, Ph. Hofmann, K.U. Weiss, R. Dippel, P. Gardner, V. Fritzsche, A.M. Bradshaw, D.P. Woodruff, M.E. Davila, M.C. Asensio, J.C. Conesa, A.R. Gonzalez-Elipe, J. Electron Spectrosc. Relat. Phenom. 64/65 (1993) 75.
[19] D.P. Woodruff, A.M. Bradshaw, Rep. Prog. Phys. 57 (1994) 1029.
[20] V. Fernandez, T. Gießel, O. Schaff, K.-M. Schindler, A. Theobald, C.J. Hirschmugl, S. Bao, A.M. Bradshaw, C. Baddeley, A.F. Lee, R.M. Lambert, D.P. Woodruff, V. Fritzsche, Z. Phys. Chem. 198 (1997) 73.
[21] E. Dietz, W. Braun, A.M. Bradshaw, R.L. Johnson, Nucl. Instrum. Methods A 239 (1985) 359.
[22] Ph. Hofmann, K.-M. Schindler, S. Bao, V. Fritzsche, A.M. Bradshaw, D.P. Woodruff, Surf. Sci. 337 (1995) 169.
[23] Ph. Hofmann, K.-M. Schindler, Phys. Rev. B 47 (1993) 13941.
[24] Ph. Hofmann, K.-M. Schindler, S. Bao, A.M. Bradshaw, D.P. Woodruff, Nature (London) 368 (1984) 131.
[25] V. Fritzsche, J. Phys. Condens. Matter 2 (1990) 1413.
[26] V. Fritzsche, Surf. Sci. 265 (1992) 187.
[27] V. Fritzsche, Surf. Sci. 213 (1986) 648.
[28] V. Fritzsche, J.B. Pendry, Phys. Rev. B 48 (1993) 9054.
[29] J.B. Pendry, J. Phys. C: Solid State Phys. 13 (1980) 937.
[30] N.A. Booth, R. Davis, R. Toomes, D.P. Woodruff, C. Hirschmugl, K.-M. Schindler, O. Schaff, V. Fernandez, A. Theobald, Ph. Hofmann, R. Lindsay, T. Gießel, P. Baumgärtel, A.M. Bradshaw, Surf. Sci. 387 (1997) 152.
[31] R. Davis, D.P. Woodruff, O. Schaff, V. Fernandez, K.-M. Schindler, Ph. Hofmann, K.-U. Weiss, R. Dippel, V. Fritzsche, A.M. Bradshaw, Phys. Rev. Lett. 74 (1995) 1621.
[32] H. Over, M. Gierer, H. Bludau, G. Ertl, Phys. Rev. B 52 (1995) 16812.
[33] C.J. Hirschmugl, K.-M. Schindler, O. Schaff, V. Fernandez, A. Theobald, P. Hofmann, A.M. Bradshaw, R. Davis, N.A. Booth, D.P. Woodruff, V. Fritzsche, Surf. Sci. 352 (1996) 232.
[34] C. Baddeley, A.F. Lee, R.M. Lambert, T. Gießel, O. Schaff, C.J. Hirschmugl, V. Fernandez, K.-M. Schindler, A. Theobald, S. Bao, A.M. Bradshaw, D.P. Woodruff, Surf. Sci. 400 (1998) 166.
[35] W.K. Kuhn, J. Szanyi, D.W. Goodman, Surf. Sci. 274 (1992) L611.
[36] J. Szanyi, W.K. Kuhn, D.W. Goodman, J. Vac. Sci. Technol. A 11 (1993) 1969.
[37] R. Toomes, O. Schaff, N.A. Booth, J.D. Denlinger, E. Rotenberg, A.M. Bradshaw, D.P. Woodruff, in: Advanced Light Source, Compendium of User Abstracts and Technical Reports 1993–1996, University of California, 1997, p. 157.